ECOLOGY

Shifting cyclone travel speed and its impact on global mangrove ecosystems

Yu Mo[1,2]*, Jim W. Hall[2], Andrew H. Baldwin[3], Marc Simard[4], Ian Donohue[1]

Cyclones cause major damage to mangrove ecosystems globally. While this damage is projected to increase as storms intensify with climate change, the consequences of changes in cyclone attributes other than wind speed remain largely unexplored. Here, we show that shifts in cyclone travel speed may also dramatically alter the risks and mechanisms of damage. By developing an interpretable machine learning model trained with all cyclones recorded worldwide from 2001 to 2021, we find that fast-moving cyclones tend to be especially destructive on steeply sloping coasts, exacerbating physical damage, whereas slow-moving cyclones induce predominantly hydrological damage. Between 1981–2000 and 2001–2020, exposure of global mangrove ecosystems to cyclones increased by 13%, accompanied by substantial changes in cyclone travel speeds, with exposure to slow- and fast-moving cyclones doubling in, respectively, the Caribbean and East Asia. Our results highlight opportunities to integrate regional shifts in cyclone attributes under a changing climate into mangrove management strategies.

INTRODUCTION

Mangrove ecosystems provide a multitude of vital services to humanity, including food provision, climate regulation, and shoreline stabilization (*1*, *2*). Their presence also confers substantial protection against cyclones to extensive tropical, subtropical, and warm temperate shorelines around the globe. Cyclones, however, also comprise a major driver of global mangrove losses (*3*, *4*), shaping mangrove productivity, structures, and functions at the global level (*5*, *6*). A thorough understanding of the complex mechanisms through which cyclones affect mangrove ecosystems is, therefore, crucial for managing and conserving these systems, particularly as cyclones are projected to intensify as the climate continues to warm (*7*, *8*).

While mangroves are generally well adapted to cyclone disturbance, cyclones still account for almost half of naturally induced mangrove mortality globally (*9*). Cyclone damage typically occurs through two mechanisms: (i) physical damage caused by cyclone forces such as winds, waves, surges, and rainfall, usually observed as canopy destruction, uprooting, and substrate erosion; and (ii) hydrological damage triggered by cyclone-induced environmental changes such as flooding, sediment smothering, and salinity stress, often manifested as diebacks (*5*). These processes can be complex. Surge inundation can, for example, shield shorter canopies from wind damage (*10*), while cyclone-induced sediment deposition can drive substantial redistribution of nutrients within and among coastal systems (*11*–*13*). Cyclone disturbance also has profound impacts on mangrove species composition and structural integrity as trees with different traits and conditions exhibit varying levels of vulnerability and follow distinct recovery pathways [e.g., (*14*–*16*)]. Thus, cyclones can affect mangrove systems in complex and variable ways, from the scale of individual trees through to community and ecosystem levels (*17*).

Recent remote sensing–based studies have greatly advanced our understanding of cyclone damage to ecosystems at large scales, enhancing our ability to estimate the consequences of observed and projected changes in global cyclone activity. For example, quantifying the effects of cyclone intensity at the regional (*18*, *19*) and global (*20*) levels has facilitated estimation of how changes in the frequency of major cyclones (that is, category 3 and above) may drive regional shifts in the risk of cyclone damage to mangroves worldwide (*8*). However, the extent and mechanisms of damage may also depend on cyclone attributes other than wind speed, such as cyclone travel speed and rainfall (*21*, *22*), whose effects remain understudied at large scales and exhibit inconsistencies (see table S1 for a detailed overview of the literature on the topic). This comprises a critical gap in our understanding that hinders our ability to assess and predict cyclone impacts on mangroves, particularly as these attributes are also expected to change as the climate continues to warm (*23*).

To address this knowledge gap, we develop an interpretable machine learning model (Fig. 1A) to explore the importance of different cyclone attributes in predicting cyclone damage to mangroves in light of ongoing climate change. Specifically, we (i) apply continuous satellite-based Earth observations [that is, MOD13Q and MYD13Q v6; (*24*)] to measure damage to global mangrove ecosystems (*25*) from historical cyclones that occurred over the past two decades [2001–2021 International Best Track Archive for Climate Stewardship, IBTrACS (*26*); category 1 and above; see Materials and Methods]. We then (ii) build a machine learning model to relate the measured damage to a range of cyclone attributes (including wind speed, travel speed, and rainfall) and coastal geomorphology, which can strongly modify cyclone forces (*21*, *27*), and (iii) construct stochastic-based response functions to quantify the effects of the predictors. Last, we (iv) analyze cyclone activity over mangrove coastlines worldwide between 1981 and 2020 to examine ongoing shifts in cyclone characteristics.

RESULTS

Damage assessment

In total, 831 discrete events (that is, cyclone-cell pairs; see Materials and Methods) were sampled from our 21-year survey period (Fig. 1B and table S2). Although the Northwest Pacific basin had the greatest cyclone activity (32% of cyclones worldwide), mangroves in

[1]School of Natural Sciences, Trinity College Dublin, Dublin, Ireland. [2]Environmental Change Institute, School of Geography and the Environment, University of Oxford, Oxford, UK. [3]Department of Environmental Science and Technology, University of Maryland, College Park, MD, USA. [4]Radar Science and Engineering Section, Jet Propulsion Laboratory, California Institute of Technology, Pasadena, CA, USA.
*Corresponding author. Email: moyu@tcd.ie

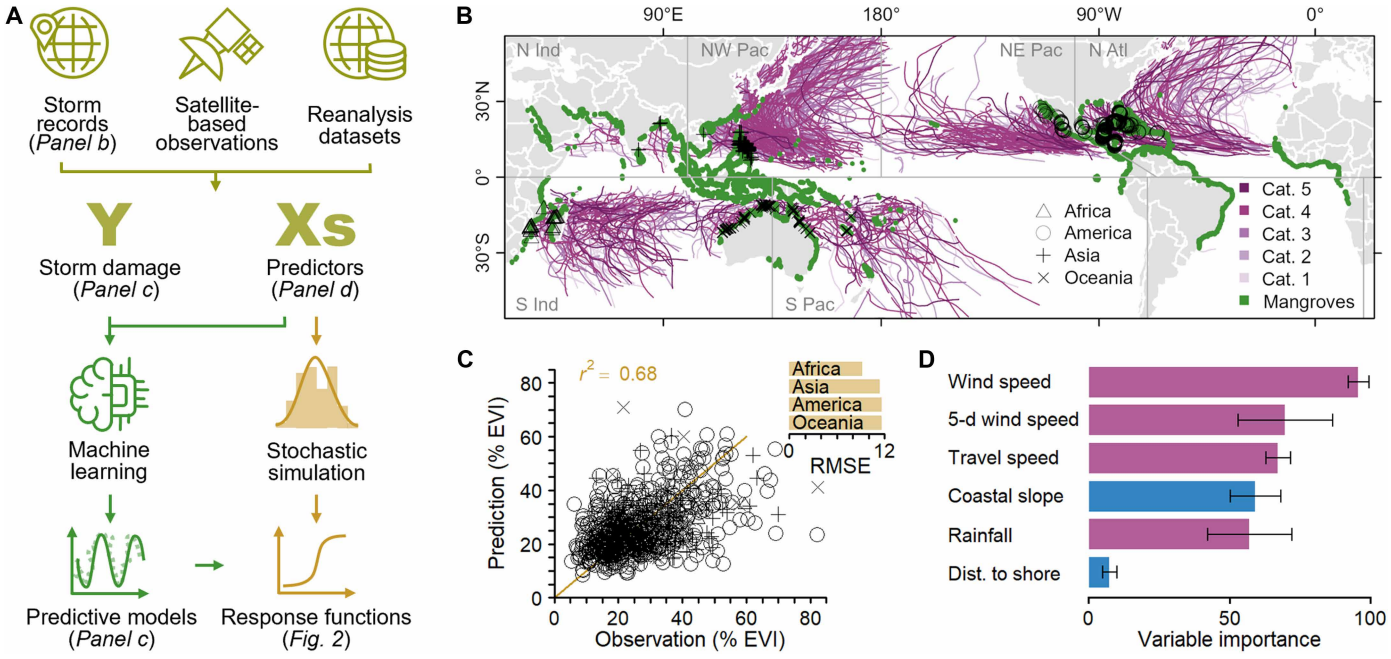

Fig. 1. Modeling cyclone damage to mangrove ecosystems. (**A**) Flowchart of our modeling approach. (**B**) Global mangrove extent (green area), tropical cyclone tracks (2001–2021; purple lines), and the locations of sampling events (that is, cyclone-cell pairs; black symbols) in Africa, America, Asia, and Oceania (triangles, circles, pluses, and crosses, respectively). (**C**) Model performance as evaluated by the coefficient of determination (r^2) and root mean square error (RMSE; inner panel). The values were computed with the leave-one-out cross-validation method (see Materials and Methods). (**D**) The relative importance of cyclone attributes (purple bars) and coastal geomorphological characteristics (blue bars) estimated by different machine learning algorithms (see Materials and Methods). Error bars represent SE.

the North Atlantic basin experienced the most frequent cyclone disturbances (33% of the mangrove-intercepting cyclones globally and 52% of the events that caused significant mangrove damage, $P < 0.05$; see Materials and Methods). The global average cyclone damage in our survey period equated to a 27 ± 12% (mean ± SD) decrease from the precyclone baseline in our measure of mangrove vegetation condition, the Enhanced Vegetation Index (EVI; see Materials and Methods). This level of damage was broadly similar across regions ($P = 0.14$; fig. S1A).

Damage modeling

We developed an ensemble machine learning model, via integrating a set of well-performing algorithms (table S3), to relate cyclone damage to six predictors, four describing cyclone attributes [that is, (local maximum sustained) wind speed, 5-day (average) wind speed, (cyclone) travel speed, and (cumulative) rainfall] and two describing coastal geomorphology [that is, coastal slope and distance (of the mangrove systems) from the shore] (table S4; see Materials and Methods). The model performed remarkably well, explaining 68% of the total variance in events worldwide (based on leave-one-out cross-validation; see Materials and Methods), and its consistency across regions is evident in similar root mean squares (Fig. 1C). On the basis of the algorithms' built-in variable importance analysis (see Materials and Methods), wind speed was the most important predictor, followed by 5-day wind speed (as an indicator of total cyclone energy), travel speed, coastal slope, rainfall, and distance from shore (Fig. 1D).

Response functions

To gain further insights into the effects of the predictors, we simulated in excess of 10,000 stochastic events—modeled events that preserve the probability distributions of predictors and the correlations among them in the historical events (fig. S2 and table S5)—to construct response functions that illustrate how cyclone damage varies as the predictors change (Fig. 2 and fig. S3). An analysis of variance (ANOVA) of the predictors revealed that the effect of coastal slope interacts with travel speed ($P = 0.001$; table S6), hence, separate response functions were developed for coastal slope under different cyclone travel speed conditions.

The response functions demonstrate positive but distinct associations between wind speed, 5-day wind speed, and travel speed and cyclone damage. Damage increased sharply when wind speed rose beyond ~100 km hour^{-1} (Fig. 2A) and showed a steady upward trend with increasing 5-day wind speed (Fig. 2B). In contrast, damage increased substantially as travel speed exceeded ~25 km hour^{-1} but remained relatively stable beyond 30 km hour^{-1} (Fig. 2C). Notably, coastal slope showed distinctive effects under different travel speeds: Damage from fast-moving cyclones (that is, cyclones with travel speed ≥25 km hour^{-1}) increased on coasts with off-shore slopes in excess of ~0.05 m m^{-1} (approximately the 75% precentile of events in Asia and the 80% precentile in America; fig. S1F). In contrast, the damage from slow-moving cyclones (travel speed <25 km hour^{-1}), while overall being lower than that from fast-moving cyclones, tended to decline as the coastal slope increased (Fig. 2D).

Changes between 1981 and 2020

To explore the impacts of ongoing changes in cyclone characteristics, we examined the number and attributes of cyclones passing over mangrove shorelines worldwide over the past four decades. At the global level, while the number of cyclones traversing mangrove ecosystems remained similar from 1981–2000 to 2001–2020 (averaging

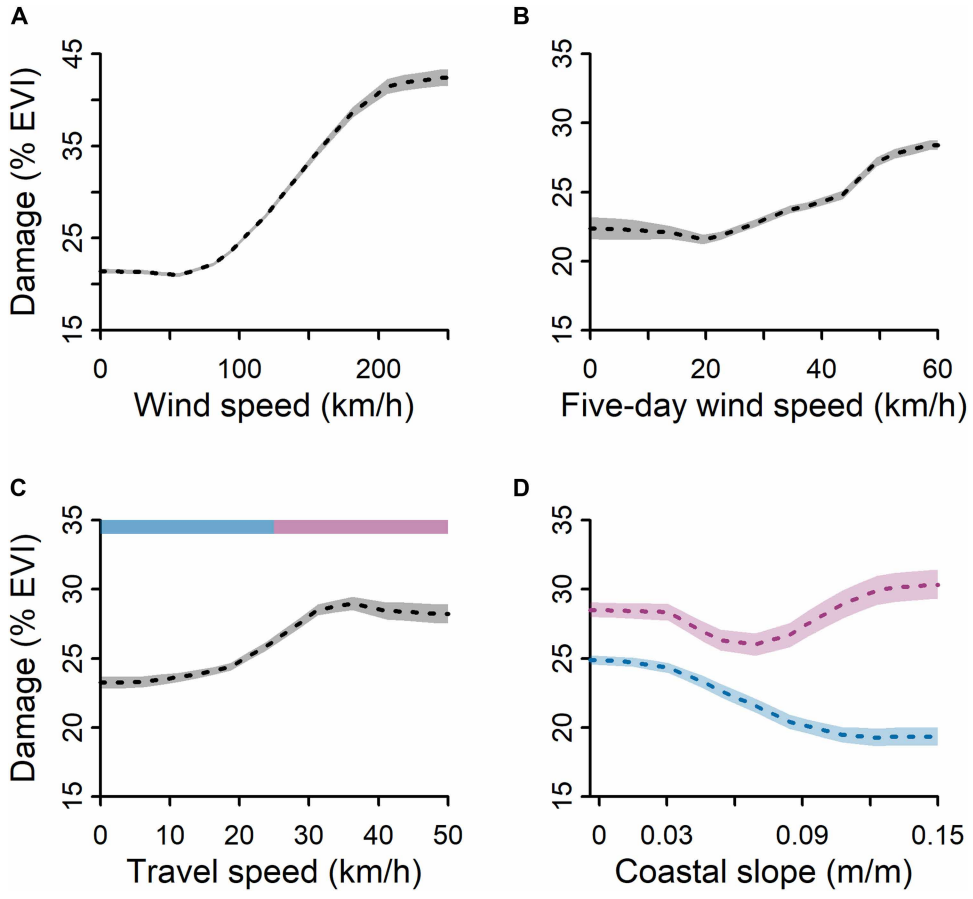

Fig. 2. Damage to mangroves as functions of cyclone attributes and coastal geomorphological conditions. Stochastic-based response functions describing the effects of (**A**) wind speed, (**B**) 5-day wind speed, (**C**) travel speed, and (**D**) coastal slope on cyclone damage. Blue and red lines in (D) correspond, respectively, to slow- (travel speed <25 km hour^{-1}) and fast-moving (travel speed ≥25 km hour^{-1}) cyclones. The dotted lines and shaded areas represent, respectively, the means and SEs of the response functions. Note the larger range of the *y* axis in (A). See table S6 for the results of statistical analyses of the predictors. h, hours.

~23 cyclones per year, $P = 0.74$; table S7), cyclone exposure (that is, cyclone track points intersecting mangrove habitats; see Materials and Methods) significantly rose by ~13% ($P < 0.001$; Fig. 3A). The ratio of mild-to-strong cyclone exposure (1.16 ± 0.43, mean ± SD) and the ratio of slow to fast-moving cyclone exposure (5.89 ± 2.74) remained relatively stable over time ($P = 0.82$ and 0.78, respectively). Nevertheless, substantial differences in the rates of change were observed (Fig. 3, B to E): Strong cyclone exposure increased at twice the rate of mild cyclones (17% compared with 9%), and fast-moving strong cyclone exposure increased at more than double the rate of slow-moving strong cyclone exposure (25% as against 11%).

Substantial shifts across basins and regions were also found (Fig. 4 and figs. S4 to S6). For example, East Asia emerged as the region facing the greatest cyclone exposure and by far the greatest strong cyclone exposure (Fig. 4, A and B), with exposure to fast-moving strong cyclones doubling over the past four decades (Fig. 4C and fig. S6C). The Caribbean became the region facing the second-greatest strong cyclone exposure (Fig. 4B), driven largely by a doubling of exposure to slow-moving strong cyclones (Fig. 4D and fig. S6D). In contrast, Australasia and Southeast Asia both experienced declines in exposure to all cyclone types (Fig. 4). Total cyclone energy (inferred from 5-day wind speed) and cyclone-induced rainfall also exhibited substantial regional shifts (table S8). For example, the North Atlantic basin experienced an 8% increase in total energy ($P = 0.05$), while East Asia and Southeast Asia saw increases of, respectively, 22 and 30% in rainfall from 1981–2000 to 2001–2020 ($P = 0.003$ and 0.001, respectively).

DISCUSSION

Our 21-year global study elucidates the influence of different cyclone attributes on the extent and mechanisms of damage to mangrove ecosystems worldwide. The interpretable machine learning model, which provides detailed response functions, greatly enhances our ability to interpret the complex and interactive effects of cyclone attributes comparedwith more traditional machine learning approaches. The model forms a robust basis for exploring the consequences of the observed changes in cyclone activity over mangrove shorelines over the past four decades, indicating substantial regional shifts in the risks and mechanisms of damage—an important phenomenon that must be considered for effective mangrove ecosystem management in a changing climate.

Our observed mean reduction of ~30% from baseline EVI at the 5-km scale is consistent with previous global assessments—e.g., ranging from 0 to 70% at the 30-m scale (*20*) and means of 5 to 20% at the 10-km scale (*8*). Our model, based on all cyclones observed

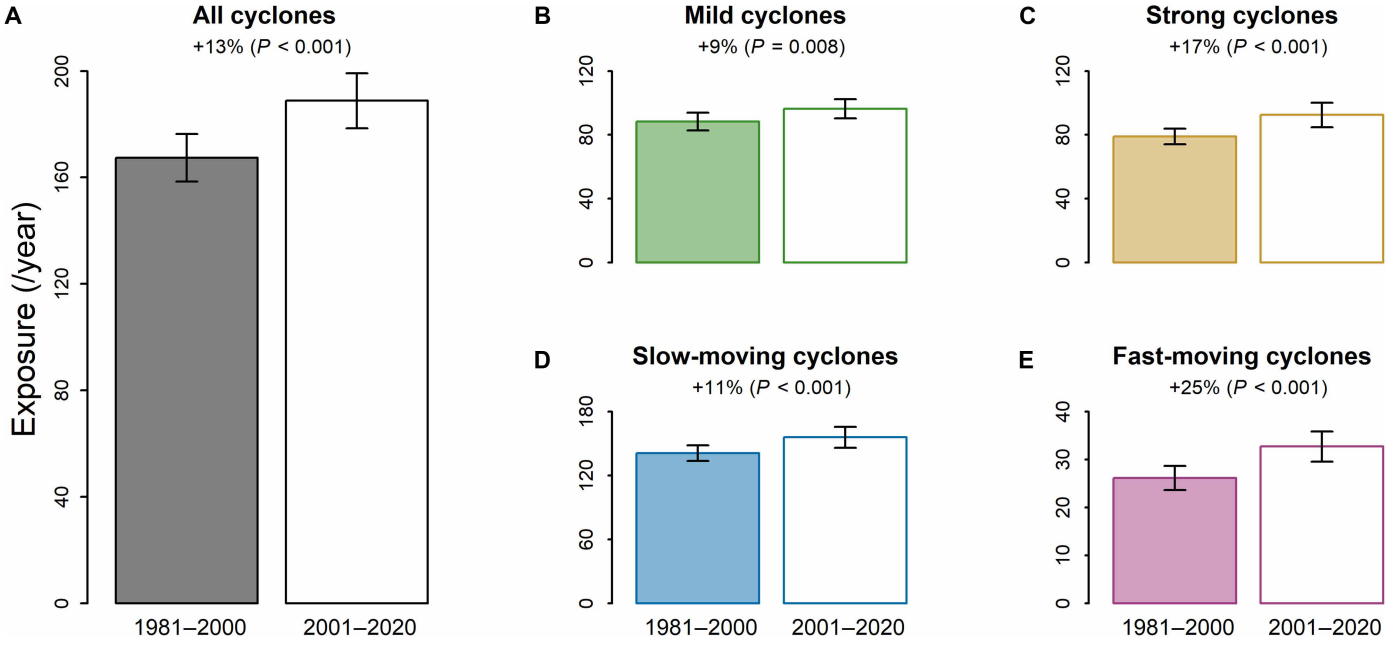

Fig. 3. Changes in exposure of global mangrove habitats to cyclones, 1981 to 2020. (**A**) Total cyclone frequency between the periods 1981–2000 and 2001–2020. Bars and error bars represent, respectively, means and SEs. Numbers on top indicate percentage changes in 2001 to 2020 relative to 1981 to 2000. (**B** to **E**) Same as (A) but for, respectively, (B) mild cyclones with wind speed <100 km hour^{-1}, (C) strong cyclones with wind speed ≥100 km hour^{-1}, (D) slow-moving cyclones with travel speed <25 km hour^{-1}, and (E) fast-moving cyclones with travel speed ≥25 km hour^{-1}.

worldwide over more than two decades, encompasses a substantially larger sample size with broader variation in cyclone attributes, as well as biotic and abiotic contexts, compared with previous regional (*18*, *19*) and global (*20*) models. It nevertheless performed very favorably in terms of variance explained (table S1), which is likely due at least partially to the capacity for machine learning to handle nonlinear and interactive predictors. The response function of wind speed shows a substantial increase in cyclone damage to mangrove ecosystems when wind speed exceeded 100 km hour^{-1}, consistent with findings from previous regional (*18*) and global (*8*) studies. In previous studies, rainfall was also found to be a positive predictor of cyclone damage in the North Atlantic region (*18*, *19*) but not a significant driver at the global scale (*20*). Our findings are consistent with the latter as rainfall's importance as a predictor ranks fifth (Fig. 1D) and its response function indicates a weak effect (fig. S3A). Heavy rainfall can lead to prolonged flooding and associated anaerobic stress in mangroves (*18*), but it may also mitigate the surge-induced salinity increases (*28*). These complex and often opposing effects make it difficult to generalize the impact of rainfall on mangroves at the global scale.

Although 5-day wind speed, as expected, correlated significantly with both wind speed and travel speed (Spearman correlation coefficients of 0.61 and −0.17, respectively, $P < 0.001$ in both cases; table S5), and all three variables were associated positively with cyclone damage, their response functions exhibit distinct patterns that offer additional insights. The more gradual relationship between total energy (inferred from 5-day wind speed) and damage suggests a cumulative effect, while the rapid increase in damage with rising wind speed and travel speed within specific ranges may reflect threshold effects related to the peak intensity and duration of cyclone forces. Moreover, our model reveals the strong influence of travel speed on damage mechanisms: Fast-moving cyclones caused higher damage on coasts with steeper slopes (>0.05 m min^{-1}) where waves penetrate closer to the shore and concentrate their energy on the shoreline (*29*). This clearly suggests a prevalence of direct physical damage such as substrate erosion, peat collapse, and shoreline retreat (*30*–*33*). On the other hand, damage from slow-moving cyclones was more apparent on gently sloping coasts where higher surges are usually generated (*34*), indicating severe indirect hydrological disturbances such as sediment smothering, low oxygen, and saline and sulfide toxicity (*21*, *22*). These mechanisms are consistent with previous studies based on specific events, primarily in Florida in the United States [e.g., (*21*, *35*, *36*)], and help to explain distinct spatial patterns of damage from the two strongest cyclones passing Florida over the past 20 years (figs. S7 and S8).

Our finding that the number of cyclones interacting with global mangrove ecosystems remained relatively constant between 1981 and 2020 aligns with previous studies showing no clear trends in global cyclone frequency or landfalls since 1970 (*37*, *38*). The observed increase in cyclone exposure—defined as cyclone track points intersecting mangrove habitats—was likely driven by a slowdown in cyclone travel speed (*37*), while the rapid increase in strong cyclone exposure may also reflect the observed increase in global average cyclone intensity (*39*). Our analysis, building on previous basin-level assessments (*5*, *17*), provides insights into sub–basin level patterns, offering a more detailed representation of the high spatial variability in cyclone activity. For example, while supporting previous studies indicating high cyclone frequency in the Northwest Pacific basin (*17*), our results show an increase in cyclone frequency in East Asia but a decrease in Southeast Asia. These changes likely reflect the poleward migration of northwest Pacific cyclones (*37*). Although both contribute to the observed increase in cyclone frequency in the

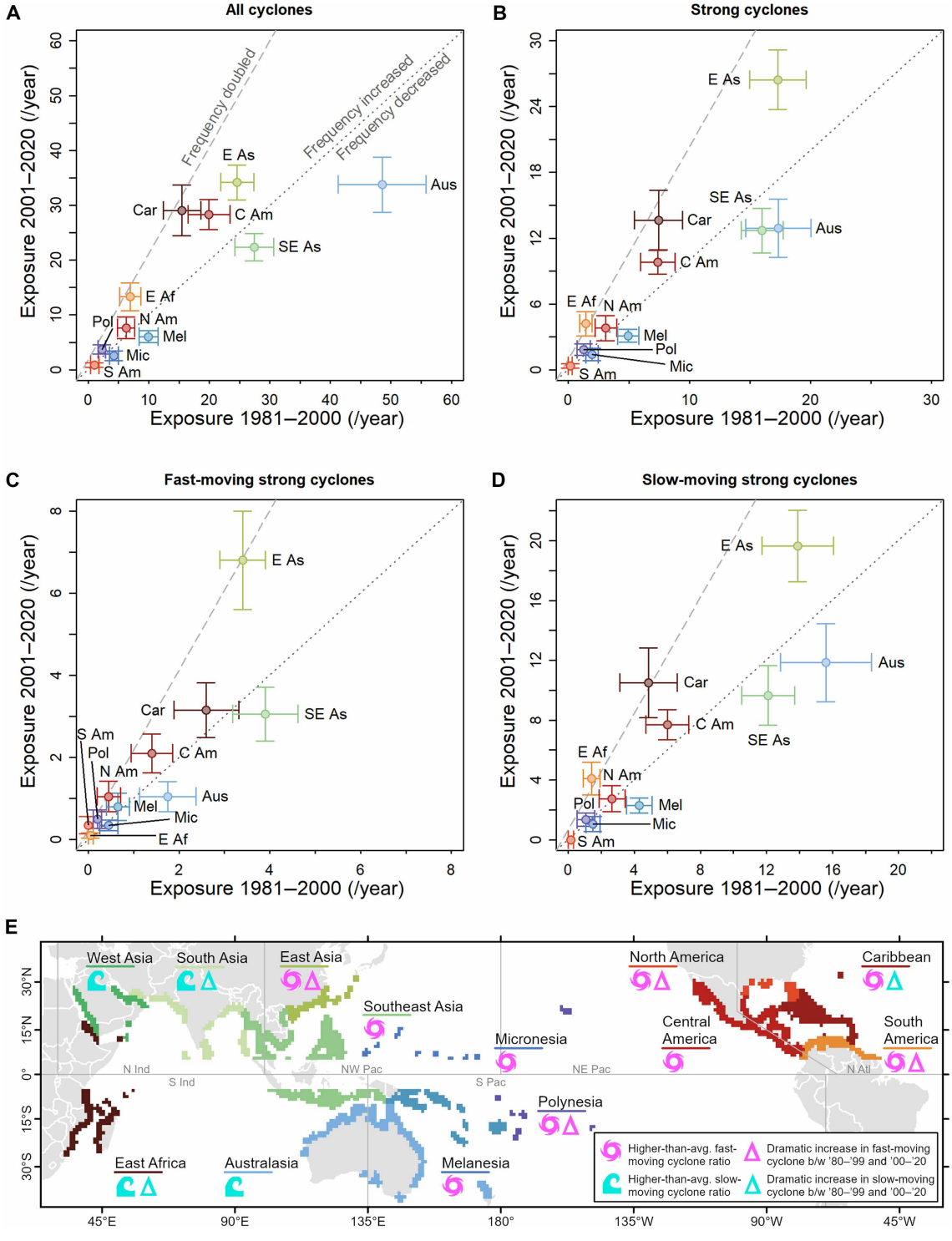

Fig. 4. Exposure of mangrove habitats to cyclone hazards worldwide. (**A**) Cyclone exposure of mangrove ecosystems worldwide in the periods 1981–2000 (*x* axis) and 2001–2020 (*y* axis). Symbols and error bars represent means and SEs. (**B** to **D**) Same as (A) but for, respectively, (B) strong cyclones with wind speed ≥100 km hour^{-1}, (C) fast-moving strong cyclones with wind speed ≥100 km hour^{-1} and travel speed ≥25 km hour^{-1}, and (D) slow-moving strong cyclones with wind speed ≥100 km hour^{-1} and travel speed <25 km hour^{-1}. The underlying data for [(A) to (D)] are detailed in table S7. (**E**) A corresponding map summarizing changing cyclone hazard risk to global mangrove systems (at 1° grid).

North Atlantic basin, the Caribbean and North America have experienced a doubling in exposure to, respectively, slow- and fast-moving cyclones. These patterns likely reflect the slowdown of North Atlantic cyclones (*37*) and the enhanced northward wind over the Gulf of Mexico (*40*). The drivers underlying the observed shifts in cyclone activity are not yet fully understood, although large-scale atmospheric circulations (such as Hadley cells) and sea surface temperature are often considered to be key players (*23*).

We used EVI to assess the biophysical properties [that is, canopy cover; (*41*)] of diverse mangrove ecosystems worldwide, given its larger dynamic range than other vegetation indices for dense vegetation (see Materials and Methods). Our results represent an average over a relatively large area (that is, 5 km by 5 km), and the damage at smaller scales could be more severe. Local cyclone damage to mangroves can be influenced by a plethora of factors, including other cyclone attributes [such as surge and wave heights, (*29*)] and coastal geomorphological features [such as terrain elevation, channel network, and sea level; (*21*, *29*, *42*, *43*)], vegetation characteristics [such as canopy structures and vegetation species, (*14*, *44*)], and human activities [such as artificial engineering structures; e.g., (*18*–*20*)]. These factors are likely to exhibit substantial spatial variation and should be better examined in future studies with higher spatial resolution. On the other hand, large-scale processes such as watershed freshwater input and groundwater table may provide additional insights into the hydrological resilience of coastal environments (*45*, *46*). Future studies may also combine various remote sensing techniques to explore additional aspects of cyclone damage, for instance, using radar data to assess changes in hydrology (*47*) and hyperspectral data to examine vegetation physiology (*48*). Investigation of complementary indicators of ecosystem resilience, such as recovery rate and patterns (*19*, *20*) following slow- and fast-moving cyclones, would further enhance our understanding of postdisturbance dynamics. Our interpretable machine learning model has the potential to incorporate additional response and predictor variables, making it a powerful tool for future studies.

Overall, our results reveal that not only is cyclone exposure of global mangrove ecosystems increasing, but this is coupled with shifts in damage mechanisms and large regional variations. This has important implications not only for mangrove ecology (*5*, *6*, *17*, *49*) but also for coastal biogeochemical cycles (*11*–*13*, *50*, *51*). The predicted poleward expansion of mangrove ecosystems in a warmer climate is likely to be increasingly influenced by cyclone-associated propagule dispersal (*49*), while also being mediated by other climate change–related processes including changes in ambient temperatures (*52*), atmospheric CO_2 (*53*), weather extremes (*54*), sea levels (*55*), ocean currents (*56*), and seawater density (*57*).

Our findings also have important implications for management. In regions experiencing frequent fast-moving cyclones, for example, prioritization should be given to protection against physical damage along relatively steep shorelines, such as erosion (*3*). The development of living oyster reefs that can effectively reduce wave heights should be promoted in such locations (*58*), whereas engineering structures such as seawalls that generally result in steepened coastal slopes should be avoided (*29*). In regions facing more frequent slow-moving cyclones, management should focus on minimizing the risk of surge-induced hydrological and biogeochemical damage, via, for example, preserving local and watershed hydrology [such as maintaining freshwater inputs and tidal exchange, (*54*)] and minimizing human disturbance [such as dyke and road construction, (*14*)]. In terms of postcyclone restoration, replanting may be prioritized after fast-moving cyclones to compensate for vegetation loss due to erosion, whereas drainage restoration is likely more critical after slow-moving cyclones to alleviate hydrological disturbances and associated physiological stress (*59*–*61*). Future risk assessments should consider changes in cyclone characteristics in addition to frequency (*8*, *62*). In principle, these recommendations are also applicable to other coastal ecosystems that have similar responses to cyclone disturbance, such as marshes (*63*). Recent studies have highlighted the immense value of coastal systems serving as nature-based solutions for cyclone protection (*2*, *64*, *65*). Enhancing the resilience of these ecosystems to cyclone activity is, therefore, crucial to promoting the resilience of the coastal environment as a whole. This need is of even greater importance given the predicted increases in the frequency and intensity of extreme cyclone events (*23*)—and their associated risks to mangroves (*62*)—as climate change accelerates.

MATERIALS AND METHODS

Tropical cyclone records

Between 1981 and 2021, IBTrACS V4 (*26*) recorded 1841 categories 1–5 tropical cyclones around the world [based on the Saffir-Simpson Wind Scale; (*66*)] (Fig. 1B and table S2). Wind speeds were all converted to the World Meteorological Organization standard 10-min average sustained wind speed [that is, wind speeds recorded in 1- or 3-min averaging periods were multiplied by a factor of 0.88, (*67*)]. Tropical cyclone damage to mangroves was studied using tropical cyclones from 2001 to 2021 that had made landfalls intercepting mangroves (that is, within 100 km). If a tropical cyclone made multiple landfalls, each landfall was considered separately. In total, 374 landfalls were identified from IBTrACS for inclusion in our study.

Global mangrove extent and condition

Global mangrove extent was delineated on the basis of the Global Mangrove Forests Distribution [GMFD, (*25*)] (Fig. 1B). The GMFD dataset was chosen because it was derived specifically from Landsat data and coincided with the start of our study period for tropical cyclone damage to mangroves (that is, 2000). Mangrove conditions were estimated using the complete series of Moderate Resolution Imaging Spectroradiometer (MODIS) EVI composite dataset [MOD13Q1 and MYD13Q1, (*24*)], which has an 8-day temporal resolution (16-day for each dataset) and a 250-m spatial resolution. MODIS-derived EVI has been demonstrated to correlate strongly with mangrove leaf area index [coefficient of determination (r^2) ~ 0.7, (*41*)], and has been applied successfully to assess cyclone damage to mangrove canopies at the global scale (*8*, *20*). Each composite is filled with data of the best quality during its acquisition window—specifically, for each pixel, cloud-free data with maximum value are selected (*24*)—and the high revisit frequency of MODIS (0.5 day) enhances the likelihood of capturing such high-quality data. The EVI layer was chosen over the Normalized Difference Vegetation Index layer in this study because EVI has higher sensitivity in dense vegetative areas, thanks to its incorporation of blue wavelengths, and is, thus, a more suitable option for a global study encompassing diverse ecosystems (*20*, *68*). Satellite data analyses were done using the Google Earth Engine.

Quantification of cyclone damage

For each tropical cyclone landfall, the area of interest was defined as a curved strip, centered on the cyclone track and aligned with the

shoreline. Each strip was set to encompass an area 0 to 100 km away from the track (that is, 200 km wide in total) and 0 to 30 km away from the shoreline [estimated using the Land Water Mask Derived L3 Global 250 m, MOD44W; (*69*)]. The size of the strip was optimized to ensure capture of the full extent of the damage, as on average a category 5 cyclone will damage mangroves 50 km away from its track (*8*), and most mangrove habitats were within 10 km of the shoreline (>95%; fig. S1F). The strip was then divided into cells of 5 km by 5 km because the coarsest resolution of the datasets used in this study is 2 km (table S4).

Within each cell, the mean EVI of all mangrove pixels was measured for 3 years. That is, from 1 year before the cyclone to 2 years afterward, and monthly means were calculated to smooth the data. We monitored mangrove conditions for 2 years after cyclones to ensure capture of the most severe damage. The measurements from the 12 months before the tropical cyclone were used to define the precyclone baselines. To better isolate cyclone damage, only cells with stable baselines (that is, with percentage SD ≤0.15) were subjected to further analysis. This threshold was selected on the basis of the phenology (that is, annual growth patterns) of mangroves from different regions of the world [e.g., (*41*, *70*–*73*)] while also helping to improve the accuracy of identifying true mangrove habitats by excluding regions dominated by coastal vegetation with stronger seasonal signals such as marshes (*70*). Measurements significantly (one-tailed test, $P < 0.05$) lower than the baseline were taken as evidence of tropical cyclone damage. Cyclone damage to mangroves was defined as the maximum reduction in EVI within the 2-year postcyclone monitoring period (*74*, *75*).

If a cell was affected by multiple cyclones within a relatively short period of time, this method would attribute the impact to the first cyclone that caused statistically significant damage (because subsequent cyclones would not have been considered as affecting mangroves with stable baselines and consequently would have been excluded from our analysis). This artifact is expected to have a limited impact on our results because the ratio of mangrove systems exposed to two or more cyclones in a given year to mangrove systems exposed to only one cyclone was very low [~6%, (*8*)].

Predictive modeling using ensemble machine learning

We acquired information on six predictor variables describing cyclone attributes and coastal geomorphology: (i) (Local maximum sustained) wind speed and (ii) 5-day (average) wind speed were derived from the IBTrACS at-track wind speed with the Holland wind model. (iii) Cyclone travel speed was extracted directly from the IBTrACS records. (iv) (Cumulative) rainfall was measured over a 5-day period centered on the landing date from the Climate Hazards Group InfraRed Precipitation with Station Data (*76*)—over 99% of storms worldwide have a precipitation duration of 5 days or fewer (*77*). (v) Distance (of the mangrove habitats) to shore with the nearby shorelines estimated using the MODIS Land Water Mask maps [MOD44W, (*69*)]. (vi) Coastal slope as the average (bedrock) elevation from the shoreline to 5 km offshore, based on the NOAA ETOPO Global Relief Model (*78*). Cyclone wind speed and rainfall are recognized as direct storm damage processes, while strong associations have been found between travel speed and storm surge height [e.g., (*20*, *79*)]. Five-day wind speed was used to infer the total energy of cyclones. Both distance to shore and coastal slope might strongly modify storm forces (*21*, *27*). Detailed procedures for deriving these variables are described in table S4. Samples with outliers in any of the variables were removed. All variables were $\log_{10}$-transformed.

To develop the ensemble model, we first tested six machine learning algorithms: gradient boosting (GBM), extreme gradient boosting (XGBoost), K nearest neighbor, random forest, recursive partitioning and regression trees (RPART), and support vector machine. The machine learning models were developed using R (packages "caret," "e1071," "xgboost," and "rpart"), and their hyperparameters are illustrated in table S3. Model performance was tested using leave-one-out cross-validation (*80*), whereby each data point was predicted by a model built with data excluding that data point, and the generalized r^2 (*81*). Predictions from the three best-performing algorithms, that is, GBM, XGBoost, and RPART, were combined using a linear regression to generate the ensemble model. The relative contribution of the predictors was evaluated using the built-in variable importance analysis of the three algorithms [which essentially measures the reduction in prediction accuracy after excluding a variable, (*82*, *83*)].

Response functions

Each historical event has a set of observed values for the six predictors, and the historical dataset as a whole contains information on the probability distribution of each predictor and the correlations among the predictors. We generated in excess of 10,000 stochastic events based on the historical events using a principal component analysis (PCA)–based stochastic optimization approach (*84*) and then derived response functions as the average predictions of all stochastic events. We chose this method over the partial dependent plot as it preserves the correlations among predictors. In this approach, permutation is performed with all the predictors simultaneously with a PCA-based perturbation, in contrast to the one-at-a-time permutation used in the Monte Carlo approach. As a result, the stochastic events preserved the (probability) distributions of the predictors and the correlations among them (fig. S2 and table S5). The stochastic events were then smoothed with the R Local Polynomial Regression Fitting (LOESS) package with a degree of 0 and a span of 0.5.

Cyclone activity changes between 1981 and 2020

The IBTrACS data recorded cyclone track points at a 6-hour interval. Cyclone frequency traversing mangrove shorelines was estimated with cyclones that had at least one track point intersecting mangrove ecosystems at 1° resolution. Cyclone exposure was defined as track points intersecting mangrove habitats. Note that one cyclone may have multiple track points intersecting mangrove habitats. Cyclone-induced rainfall was estimated within a 5-km radius of the landfall track point over a 5-day period centered on the landfall date. To assess changes in cyclone activity between the periods 1981–2000 and 2001–2020, we used Poisson tests to evaluate differences in cyclone exposure and chi-squared tests to compare ratios of exposure to mild versus strong cyclones (wind speed $<$ and $\geq$ 100 km hour^{-1}, respectively) and to slow- versus fast-moving cyclones (travel speed $<$ and $\geq$ 25 km hour^{-1}, respectively). Nonparametric Wilcoxon tests were applied to compare the 5-day wind speed and rainfall distributions between the two periods.

Supplementary Materials

This PDF file includes:

Figs. S1 to S8
Tables S1 to S8
References

REFERENCES AND NOTES

1. J. Su, D. A. Friess, A. Gasparatos, A meta-analysis of the ecological and economic outcomes of mangrove restoration. *Nat. Commun.* **12**, 5050 (2021).
2. V. T. M. van Zelst, J. T. Dijkstra, B. K. van Wesenbeeck, D. Eilander, E. P. Morris, H. C. Winsemius, P. J. Ward, M. B. de Vries, Cutting the costs of coastal protection by integrating vegetation in flood defences. *Nat. Commun.* **12**, 6533 (2021).
3. V. Hagger, T. A. Worthington, C. E. Lovelock, M. F. Adame, T. Amano, B. M. Brown, D. A. Friess, E. Landis, P. J. Mumby, T. H. Morrison, K. R. O'Brien, K. A. Wilson, C. Zganjar, M. I. Saunders, Drivers of global mangrove loss and gain in social-ecological systems. *Nat. Commun.* **13**, 6373 (2022).
4. L. Goldberg, D. Lagomasino, N. Thomas, T. Fatoyinbo, Global declines in human-driven mangrove loss. *Glob. Chang. Biol.* **26**, 5844–5855 (2020).
5. K. W. Krauss, M. J. Osland, Tropical cyclones and the organization of mangrove forests: A review. *Ann. Bot.* **125**, 213–234 (2019).
6. M. Simard, L. Fatoyinbo, C. Smetanka, V. H. Rivera-Monroy, E. Castañeda-Moya, N. Thomas, T. Van der Stocken, Mangrove canopy height globally related to precipitation, temperature and cyclone frequency. *Nat. Geosci.* **12**, 40–45 (2019).
7. R. D. Ward, D. A. Friess, R. H. Day, R. A. Mackenzie, Impacts of climate change on mangrove ecosystems: A region by region overview. *Ecosyst. Health. Sustain.* **2**, e01211 (2016).
8. Y. Mo, M. Simard, J. W. Hall, Tropical cyclone risk to global mangrove ecosystems: Potential future regional shifts. *Front. Ecol. Environ.* **21**, 269–274 (2023).
9. J. Z. Sippo, C. E. Lovelock, I. R. Santos, C. J. Sanders, D. T. Maher, Mangrove mortality in a changing climate: An overview. *Estuar. Coast. Shelf Sci.* **215**, 241–249 (2018).
10. A. R. Armitage, C. A. Weaver, J. S. Kominoski, S. C. Pennings, Resistance to hurricane effects varies among wetland vegetation types in the marsh–mangrove ecotone. *Estuaries Coast.* **43**, 960–970 (2020).
11. E. Castaneda-Moya, V. H. Rivera-Monroy, R. M. Chambers, X. Zhao, L. Lamb-Wotton, A. Gorsky, E. E. Gaiser, T. G. Troxler, J. S. Kominoski, M. Hiatt, Hurricanes fertilize mangrove forests in the Gulf of Mexico (Florida Everglades, USA). *Proc. Natl. Acad. Sci. U.S.A.* **117**, 4831–4841 (2020).
12. A. J. West, C. W. Lin, T. C. Lin, R. G. Hilton, S. H. Liu, C. T. Chang, K. C. Lin, A. Galy, R. B. Sparkes, N. Hovius, Mobilization and transport of coarse woody debris to the oceans triggered by an extreme tropical storm. *Limnol. Oceanogr.* **56**, 77–85 (2011).
13. J. L. Breithaupt, J. M. Smoak, T. S. Bianchi, D. R. Vaughn, C. J. Sanders, K. R. Radabaugh, M. J. Osland, L. C. Feher, J. C. Lynch, D. R. Cahoon, G. H. Anderson, K. R. T. Whelan, B. E. Rosenheim, R. P. Moyer, L. G. Chambers, Increasing rates of carbon burial in southwest Florida coastal wetlands. *J. Geophys. Res. Biogeosciences* **125**, e2019JG005349 (2020).
14. R. Walcker, C. Laplanche, M. Herteman, L. Lambs, F. Fromard, Damages caused by hurricane Irma in the human-degraded mangroves of Saint Martin (Caribbean). *Sci. Rep.* **9**, 18971 (2019).
15. E. Asbridge, R. Lucas, K. Rogers, A. Accad, The extent of mangrove change and potential for recovery following severe tropical cyclone Yasi, Hinchinbrook Island, Queensland, Australia. *Ecol. Evol.* **8**, 10416–10434 (2018).
16. V. H. Rivera-Monroy, T. M. Danielson, E. Castañeda-Moya, B. D. Marx, R. Travieso, X. Zhao, E. E. Gaiser, L. M. Farfan, Long-term demography and stem productivity of Everglades mangrove forests (Florida, USA): Resistance to hurricane disturbance. *For. Ecol. Manage.* **440**, 79–91 (2019).
17. T.-C. Lin, J. A. Hogan, C.-T. Chang, Tropical cyclone ecology: A scale-link perspective. *Trends Ecol. Evol.* **35**, 594–604 (2020).
18. P. J. Taillie, R. Roman-Cuesta, D. Lagomasino, M. Cifuentes-Jara, T. Fatoyinbo, L. E. Ott, B. Poulter, Widespread mangrove damage resulting from the 2017 Atlantic mega hurricane season. *Environ. Res. Lett.* **15**, 064010 (2020).
19. C. Amaral, B. Poulter, D. Lagomasino, T. Fatoyinbo, P. Taillie, G. Lizcano, S. Canty, J. A. H. Silveira, C. Teutli-Hernandez, M. Cifuentes-Jara, S. P. Charles, C. S. Moreno, J. D. Gonzalez-Trujillo, R. M. Roman-Cuesta, Drivers of mangrove vulnerability and resilience to tropical cyclones in the North Atlantic Basin. *Sci. Total Environ.* **898**, 165413 (2023).
20. J. Peereman, J. A. Hogan, T. C. Lin, Disturbance frequency, intensity and forest structure modulate cyclone-induced changes in mangrove forest canopy cover. *Glob. Ecol. Biogeogr.* **31**, 37–50 (2022).
21. D. Lagomasino, T. Fatoyinbo, E. Castaneda-Moya, B. D. Cook, P. M. Montesano, C. S. R. Neigh, L. A. Corp, L. E. Ott, S. Chavez, D. C. Morton, Storm surge and ponding explain mangrove dieback in southwest Florida following hurricane Irma. *Nat. Commun.* **12**, 4003 (2021).
22. K. R. Radabaugh, R. P. Moyer, A. R. Chappel, E. E. Dontis, C. E. Russo, K. M. Joyse, M. W. Bownik, A. H. Goeckner, N. S. Khan, Mangrove damage, delayed mortality, and early recovery following hurricane Irma at two landfall sites in southwest Florida, USA. *Estuaries Coast.* **43**, 1104–1118 (2020).
23. S. I. Seneviratne, X. Zhang, M. Adnan, W. Badi, C. Dereczynski, A. Di Luca, S. M. Vicente-Serrano, M. Wehner, B. Zhou, IPCC6 "Chapter 11: Weather and climate extreme events in a changing climate" in *Climate Change 2021: The Physical Science Basis. Contribution of Working Group I to the Sixth Assessment Report of the Intergovernmental Panel on Climate Change*, V. Masson-Delmotte, P. Zhai, A. Pirani, S. L. Connors, C. Péan, S. Berger, N. Caud, Y. Chen, L. Goldfarb, M.I. Gomis, M. Huang, K. Leitzell, E. Lonnoy, J. B. R. Matthews, T.K. Maycock, T. Waterfield, O. Yelekçi, R. Yu, and B. Zhou (Eds.). (Cambridge Univ. Press, 2021), pp. 1513–1766. doi: 10.1017/9781009157896.013.
24. K. Didan, A. B. Munoz, R. Solano, A. Huete, MODIS vegetation index user's guide (MOD13 series). University of Arizona: Vegetation Index and Phenology Lab, 2015.
25. C. Giri, E. Ochieng, L. L. Tieszen, Z. Zhu, A. Singh, T. Loveland, J. Masek, N. Duke, Status and distribution of mangrove forests of the world using earth observation satellite data. *Glob. Ecol. Biogeogr.* **20**, 154–159 (2011).
26. K. R. Knapp, H. J. Diamond, J. P. Kossin, M. C. Kruk, C. J. Schreck, International Best Track Archive for Climate Stewardship (IBTrACS) Project, Version 4. NOAA National Centers for Environmental Information, 2018.
27. J. L. Irish, D. T. Resio, J. J. Ratcliff, The influence of storm size on hurricane surge. *J. Phys. Oceanogr.* **38**, 2003–2013 (2008).
28. J. R. Walker, A. C. Woods, M. K. Pierce, J. L. Steichen, A. Quigg, K. Kaiser, J. M. Labonté, Functionally diverse microbial communities show resilience in response to a record-breaking rain event. *ISME Commun.* **2**, 81 (2022).
29. R. Almar, R. Ranasinghe, E. W. J. Bergsma, H. Diaz, A. Melet, F. Papa, M. Vousdoukas, P. Athanasiou, O. Dada, L. P. Almeida, E. Kestenare, A global analysis of extreme coastal water levels with implications for potential coastal overtopping. *Nat. Commun.* **12**, 3775 (2021).
30. C. D. Woodroffe, Response of tide-dominated mangrove shorelines in Northern Australia to anticipated sea-level rise. *Earth Surf. Process. Landf.* **20**, 65–85 (1995).
31. R. Bhargava, D. Sarkar, D. A. Friess, A cloud computing-based approach to mapping mangrove erosion and progradation: Case studies from the Sundarbans and French Guiana. *Estuar. Coast. Shelf Sci.* **248**, 106798 (2021).
32. E. I. Paling, H. T. Kobryn, G. Humphreys, Assessing the extent of mangrove change caused by cyclone Vance in the eastern Exmouth Gulf, northwestern Australia. *Estuar. Coast. Shelf Sci.* **77**, 603–613 (2008).
33. D. R. Cahoon, P. Hensel, J. Rybczyk, K. L. McKee, C. E. Proffitt, B. C. Perez, Mass tree mortality leads to mangrove peat collapse at Bay Islands, Honduras after hurricane Mitch. *J. Ecol.* **91**, 1093–1105 (2003).
34. S. R. Signorini, J. S. Wei, C. D. Miller, Hurricane-induced surge and currents on the Texas-Louisiana shelf. *J. Geophys. Res.* **97**, 2229–2242 (1992).
35. H. Liu, K. Zhang, Y. Li, L. Xie, Numerical study of the sensitivity of mangroves in reducing storm surge and flooding to hurricane characteristics in southern Florida. *Cont. Shelf Res.* **64**, 51–65 (2013).
36. T. V. Wamsley, M. A. Cialone, J. M. Smith, J. H. Atkinson, J. D. Rosati, The potential of wetlands in reducing storm surge. *Ocean Eng.* **37**, 59–68 (2010).
37. T. Knutson, S. J. Camargo, J. C. L. Chan, K. Emanuel, C.-H. Ho, J. Kossin, M. Mohapatra, M. Satoh, M. Sugi, K. Walsh, L. Wu, Tropical cyclones and climate change assessment: Part I: Detection and attribution. *Bull. Am. Meteorol. Soc.* **100**, 1987–2007 (2019).
38. S. S. Chand, K. J. E. Walsh, S. J. Camargo, J. P. Kossin, K. J. Tory, M. F. Wehner, J. C. L. Chan, P. J. Klotzbach, A. J. Dowdy, S. S. Bell, H. A. Ramsay, H. Murakami, Declining tropical cyclone frequency under global warming. *Nat. Clim. Chang.* **12**, 655–661 (2022).
39. A. H. Sobel, S. J. Camargo, T. M. Hall, C.-Y. Lee, M. K. Tippett, A. A. Wing, Human influence on tropical cyclone intensity. *Science* **353**, 242–246 (2016).
40. P. Hassanzadeh, C. Y. Lee, E. Nabizadeh, S. J. Camargo, D. Ma, L. Y. Yeung, Effects of climate change on the movement of future landfalling Texas tropical cyclones. *Nat. Commun.* **11**, 3319 (2020).
41. S. Shrestha, I. Miranda, A. Kumar, M. L. E. Pardo, S. Dahal, T. Rashid, C. Remillard, D. R. Mishra, Identifying and forecasting potential biophysical risk areas within a tropical mangrove ecosystem using multi-sensor data. *I. J. Appl. Earth Obs. Geoinf.* **74**, 281–294 (2019).
42. S. Muis, M. Verlaan, H. C. Winsemius, J. C. J. H. Aerts, P. J. Ward, A global reanalysis of storm surges and extreme sea levels. *Nat. Commun.* **7**, 11969 (2016).
43. M. Mishra, T. Acharyya, C. A. G. Santos, R. M. da Silva, D. Kar, A. H. Mustafa Kamal, S. Raulo, Geo-ecological impact assessment of severe cyclonic storm Amphan on Sundarban mangrove forest using geospatial technology. *Estuar. Coast. Shelf Sci.* **260**, 107486 (2021).
44. D. Imbert, Hurricane disturbance and forest dynamics in east Caribbean mangroves. *Ecosphere* **9**, e02231 (2018).
45. X. Li, Z. Liu, S. Wang, F. Li, H. Li, T. Zhu, Z. Qian, Y. Tu, Y. Liu, X. Wang, Q. Wang, W. Shi, D. Li, Spatial characteristics of the stability of mangrove ecosystems in freshwater and seawater floods in Southeast Asia. *J. Geogr. Sci.* **32**, 1831–1846 (2022).
46. Y. Zhang, W. Li, G. Sun, J. S. King, Coastal wetland resilience to climate variability: A hydrologic perspective. *J. Hydrol.* **568**, 275–284 (2019).
47. T. T. Lê, J.-L. Froger, Multiscale framework for rapid change analysis from SAR image time series: Case study of flood monitoring in the central coast regions of Vietnam. *Remote Sens. Environ.* **269**, 112837 (2022).
48. C. Song, B. L. White, B. W. Heumann, Hyperspectral remote sensing of salinity stress on red (Rhizophora mangle) and white (Laguncularia racemosa) mangroves on Galapagos Islands. *Remote Sens. Lett.* **2**, 221–230 (2011).

49. T. Van der Stocken, A. K. S. Wee, D. J. R. De Ryck, B. Vanschoenwinkel, D. A. Friess, F. Dahdouh-Guebas, M. Simard, N. Koedam, E. L. Webb, A general framework for propagule dispersal in mangroves. *Biol. Rev. Camb. Philos. Soc.* **94**, 1547–1575 (2019).
50. T. A. M. Pugh, A. Arneth, M. Kautz, B. Poulter, B. Smith, Important role of forest disturbances in the global biomass turnover and carbon sinks. *Nat. Geosci.* **12**, 730–735 (2019).
51. L. C. Feher, M. J. Osland, G. H. Anderson, W. C. Vervaeke, K. W. Krauss, K. R. T. Whelan, K. M. Balentine, G. Tiling-Range, T. J. Smith, D. R. Cahoon, The long-term effects of Hurricanes Wilma and Irma on soil elevation change in everglades mangrove forests. *Ecosystems* **23**, 917–931 (2020).
52. N. Saintilan, N. C. Wilson, K. Rogers, A. Rajkaran, K. W. Krauss, Mangrove expansion and salt marsh decline at mangrove poleward limits. *Glob. Chang. Biol.* **20**, 147–157 (2014).
53. Z. Zhang, X. Luo, D. A. Friess, S. Wang, Y. Li, Y. Li, Stronger increases but greater variability in global mangrove productivity compared to that of adjacent terrestrial forests. *Nat. Ecol. Evol.* **8**, 239–250 (2024).
54. D. A. Sánchez-Núñez, J. A. Rodríguez-Rodríguez, J. E. Mancera Pineda, Effects of climate variability and hydrological rehabilitation measures on long-term mangrove trajectories: From reproduction to recruitment and landscape cover changes. *J. Appl. Ecol.* **60**, 2508–2520 (2023).
55. J. C. Ellison, K. Buffington, K. M. Thorne, D. B. Gesch, J. Irwin, J. J. Danielson, *Elevations of Mangrove Forests of Pohnpei, Micronesia* (Estuarine, Coastal and Shelf Science, 2022), vol. 268, pp.107780.
56. L. P. Gouvêa, E. Fragkopoulou, K. Cavanaugh, E. A. Serrao, M. B. Araújo, M. J. Costello, E. H. T. Westergerling, J. Assis, Oceanographic connectivity explains the intra-specific diversity of mangrove forests at global scales. *Proc. Natl. Acad. Sci. U.S.A.* **120**, e2209637120 (2023).
57. T. Van der Stocken, B. Vanschoenwinkel, D. Carroll, K. C. Cavanaugh, N. Koedam, Mangrove dispersal disrupted by projected changes in global seawater density. *Nat. Clim. Change* **12**, 685–691 (2022).
58. S. B. Scyphers, S. P. Powers, K. L. Heck Jr., D. Byron, Oyster reefs as natural breakwaters mitigate shoreline loss and facilitate fisheries. *PLOS ONE* **6**, e22396 (2011).
59. Q. He, Z. Li, P. Daleo, J. S. Lefcheck, M. S. Thomsen, J. B. Adams, T. J. Bouma, Coastal wetland resilience through local, regional and global conservation. *Nat. Rev. Biodivers.* **1**, 50–67 (2025).
60. S. Y. Lee, S. Hamilton, E. B. Barbier, J. Primavera, R. R. Lewis III, Better restoration policies are needed to conserve mangrove ecosystems. *Nat. Ecol. Evol.* **3**, 870–872 (2019).
61. S. D. Sasmito, M. Basyuni, A. Kridalaksana, M. F. Saragi-Sasmito, C. E. Lovelock, D. Murdiyarso, Challenges and opportunities for achieving sustainable development goals through restoration of Indonesia's mangroves. *Nat. Ecol. Evol.* **7**, 62–70 (2023).
62. S. Hülsen, L. E. Dee, C. M. Kropf, S. Meiler, D. N. Bresch, Mangroves and their services are at risk from tropical cyclones and sea level rise under climate change. *Commun. Earth Environ.* **6**, 6 (2025).
63. C. J. Patrick, J. S. Kominoski, W. H. McDowell, B. Branoff, D. Lagomasino, M. Leon, E. Hensel, M. J. S. Hensel, B. A. Strickland, T. M. Aide, A. Armitage, M. Campos-Cerqueira, V. M. Congdon, T. A. Crowl, D. J. Devlin, S. Douglas, B. E. Erisman, R. A. Feagin, S. J. Geist, N. S. Hall, A. K. Hardison, M. R. Heithaus, J. A. Hogan, J. D. Hogan, S. Kinard, J. J. Kiszka, T.-C. Lin, K. Lu, C. J. Madden, P. A. Montagna, C. S. O'Connell, C. E. Proffitt, B. K. Reese, J. W. Reustle, K. L. Robinson, S. A. Rush, R. O. Santos, A. Schnetzer, D. L. Smee, R. S. Smith, G. Starr, B. A. Stauffer, L. M. Walker, C. A. Weaver, M. S. Wetz, E. R. Whitman, S. S. Wilson, J. Xue, X. Zou, A general pattern of trade-offs between ecosystem resistance and resilience to tropical cyclones. *Sci. Adv.* **8**, eabl9155 (2022).
64. R. Costanza, S. J. Anderson, P. Sutton, K. Mulder, O. Mulder, I. Kubiszewski, X. Wang, X. Liu, O. Pérez-Maqueo, M. Luisa Martinez, D. Jarvis, G. Dee, The global value of coastal wetlands for storm protection. *Glob. Environ. Chang.* **70**, 102328 (2021).
65. L. T. M. Huynh, J. Su, Q. Wang, L. C. Stringer, A. D. Switzer, A. Gasparatos, Meta-analysis indicates better climate adaptation and mitigation performance of hybrid engineering-natural coastal defence measures. *Nat. Commun.* **15**, 2870 (2024).
66. National Oceanic and Atmospheric Administration (NOAA), Saffir-Simpson Hurricane Wind Scale. 2021.
67. B. A. Harper, J.D. Kepert, J.D. Ginger, *Guidelines for Converting between Various Wind Averaging Periods in Tropical Cyclone Conditions* (World Meteorological Organization, 2010).
68. A. Huete, K. Didan, T. Miura, E. P. Rodriguez, X. Gao, L. G. Ferreira, Overview of the radiometric and biophysical performance of the MODIS vegetation indices. *Remote Sens. Environ.* **83**, 195–213 (2002).
69. M. Carroll, C. DiMiceli, M. Wooten, A. Hubbard, R. Sohlberg, J. Townshend, MOD44W MODIS/Terra Land Water Mask Derived from MODIS and SRTM L3 Global 250m SIN Grid V006, N.E.L.P. DAAC, Editor. 2017.
70. H. Li, M. Jia, R. Zhang, Y. Ren, X. Wen, Incorporating the plant phenological trajectory into mangrove species mapping with dense time series sentinel-2 imagery and the Google Earth engine platform. *Remote Sens* **11**, 11 (2019).
71. J. Pastor-Guzman, J. Dash, P. M. Atkinson, Remote sensing of mangrove forest phenology and its environmental drivers. *Remote Sens. Environ.* **205**, 71–84 (2018).
72. J. Long, C. Giri, J. Primavera, M. Trivedi, Damage and recovery assessment of the Philippines' mangroves following super typhoon Haiyan. *Mar. Pollut. Bull.* **109**, 734–743 (2016).
73. K. Zhang, B. Thapa, M. Ross, D. Gann, Remote sensing of seasonal changes and disturbances in mangrove forest: A case study from South Florida. *Ecosphere* **7**, e01366 (2016).
74. L. White, N. E. O'Connor, Q. Yang, M. C. Emmerson, I. Donohue, Individual species provide multifaceted contributions to the stability of ecosystems. *Nat. Ecol. Evol.* **4**, 1594–1601 (2020).
75. Q. Yang, M. S. Fowler, A. L. Jackson, I. Donohue, The predictability of ecological stability in a noisy world. *Nat. Ecol. Evol.* **3**, 251–259 (2019).
76. C. Funk, P. Peterson, M. Landsfeld, D. Pedreros, J. Verdin, S. Shukla, G. Husak, J. Rowland, L. Harrison, A. Hoell, The climate hazards infrared precipitation with stations—A new environmental record for monitoring extremes. *Sci. Data* **2**, 150066 (2015).
77. R. H. White, D. S. Battisti, G. Skok, Tracking precipitation events in time and space in gridded observational data. *Geophys. Res. Lett.* **44**, 8637–8646 (2017).
78. NOAA National Geophysical Data Center, ETOPO1 1 Arc-Minute Global Relief Model, N.N.C.f.E. Information, Editor. 2009.
79. K. Zhang, H. Liu, Y. Li, H. Xu, J. Shen, J. Rhome, T. J. Smith, The role of mangroves in attenuating storm surges. *Estuar. Coast. Shelf Sci.* **102-103**, 11–23 (2012).
80. L. A. Yates, Z. Aandahl, S. A. Richards, B. W. Brook, Cross validation for model selection: A review with examples from ecology. *Ecological monographs* **93**, e1557 (2023).
81. S. Nakagawa, H. Schielzeth, A general and simple method for obtaining R^2 from generalized linear mixed-effects models. *Methods Ecol. Evol.* **4**, 133–142 (2013).
82. T. M. Therneau, E. J. Atkinson, An introduction to recursive partitioning using the RPART routines, in Mayo Foundation: Technical report. 2022.
83. M. Kuhn, Variable importance using the caret package. 2007.
84. A. Kuznetsova, G. Pons-Moll, B. Rosenhahn, *PCA-enhanced stochastic optimization methods, in oint DAGM (German Association for Pattern Recognition) and OAGM Symposium* (Springer, 2012), pp. 377–386.
85. T. J. Smith, G. H. Anderson, K. Balentine, G. Tiling, G. A. Ward, K. R. T. Whelan, Cumulative impacts of hurricanes on Florida mangrove ecosystems: Sediment deposition, storm surges and vegetation. *Wetlands* **29**, 24–34 (2009).
86. J. Svejkovsky, D. E. Ogurcak, M. S. Ross, A. Arkowitz, Satellite image-based time series observations of vegetation response to hurricane Irma in the lower Florida Keys. *Estuaries Coasts* **43**, 1058–1069 (2020).
87. Mohammed, F. Sultana, A. Khan, S. Ahammed, S. R. Saimun, S. Bhuiyan, S. K. Srivastava, S. A. Mukul, M. A. S. Arfin-Khan, Assessing vulnerability to cyclone hazards in the World's largest mangrove forest, the Sundarbans: A geospatial analysis. *Forests* **15**, 1722 (2024).
88. M. Mishra, T. Acharyya, B. Halder, C. A. G. Santos, R. M. da Silva, N. R. Rout, D. Bhattacharyya, Impact assessment of cyclone Yaas on the mangrove forest area in the Bhitarkanika National Park (India). *J. Mar. Syst.* **242**, 103947 (2024).
89. C. J. Feehan, K. Filbee-Dexter, M. S. Thomsen, T. Wernberg, T. Miles, Ecosystem damage by increasing tropical cyclones. *Commun. Earth Environ.* **5**, 5 (2024).
90. Y. Mo, Can space-borne SAR be applied to salt marshes? A case study comparing UVA and Sentinel-1. (American Geophysical Union Fall Meeting, 2023).
91. C. Zhang, S. D. Durgan, D. Lagomasino, Modeling risk of mangroves to tropical cyclones: A case study of hurricane Irma. *Estuar. Coast. Shelf Sci.* **224**, 108–116 (2019).
92. T. M. Danielson, V. H. Rivera-Monroy, E. Castañeda-Moya, H. Briceño, R. Travieso, B. D. Marx, E. Gaiser, L. M. Farfán, Assessment of Everglades mangrove forest resilience: Implications for above-ground net primary productivity and carbon dynamics. *For. Ecol. Manage.* **404**, 115–125 (2017).
93. C. C. F. Macamo, E. Massuanganhe, D. K. Nicolau, S. O. Bandeira, J. B. Adams, Mangrove's response to cyclone Eline (2000): What is happening 14 years later. *Aquat. Bot.* **134**, 10–17 (2016).
94. T. T. Aung, M. M. Than, O. Katsuhiro, M. Yukira, Assessing the status of three mangrove species restored by the local community in the cyclone-affected area of the Ayeyarwady Delta, Myanmar. *Wetlands Ecol. Manage.* **19**, 195–208 (2011).
95. J. Rogan, L. Schneider, Z. Christman, M. Millones, D. Lawrence, B. Schmook, Hurricane disturbance mapping using MODIS EVI data in the southeastern Yucatán, Mexico. *Remote Sens. Lett.* **2**, 259–267 (2011).
96. T. W. Doyle, K. W. Krauss, C. J. Wells, Landscape analysis and pattern of hurricane impact and circulation on mangrove forests of the Everglades. *Wetlands* **29**, 44–53 (2009).
97. K. Zhang, M. Simard, M. Ross, V. H. Rivera-Monroy, P. Houle, P. Ruiz, R. R. Twilley, K. Whelan, Airborne laser scanning quantification of disturbances from hurricanes and lightning strikes to mangrove forests in Everglades National Park, USA. *Sensors* **8**, 2262–2292 (2008).
98. M. S. Ross, P. L. Ruiz, J. P. Sah, D. L. Reed, J. Walters, J. F. Meeder, Early post-hurricane stand development in Fringe mangrove forests of contrasting productivity. *Plant Ecol.* **185**, 283–297 (2006).

99. R. E. Sherman, T. J. Fahey, P. Martinez, Hurricane impacts on a mangrove forest in the Dominican Republic: Damage patterns and early recovery. *Biotropica* **33**, 393–408 (2001).
100. A. H. Baldwin, W. J. Platt, K. L. Gathen, J. M. Lessmann, T. J. Rauch, Hurricane damage and regeneration in fringe mangrove forests of southeast Florida, USA. *J. Coast. Res.* , 169–183 (1995).
101. T. W. Doyle, T. J. Smith III, M. B. Robblee, Wind damage effects of hurricane Andrew on mangrove communities along the southwest coast of Florida, USA. *J. Coast. Res.* **21**, 159–168 (1995).
102. N. Lin, D. Chavas, On hurricane parametric wind and applications in storm surge modeling. *J. Geophys. Res. Atmos.* **117**, 117 (2012).
103. J. Butke, The Pressure's On: Increased realism in tropical cyclone wind speeds through attention to environmental pressure, in *AIR Currents* 2012.
104. H. E. Graham, G. N. Hudson, Surface winds near the center of hurricanes (and other cyclones), in *National Hurricane Research Project. 1960*, Hydrometeorological Section, Hydrologic Services Division, U. S. Weather Bureau: Washington D. C.
105. E. Rapaport, Preliminary report: Hurricane Andrew 16–28 August 1992. 1993.
106. R. J. Pasch, E. S. Blake, H. D. I. Cobb, D. P. Roberts, Tropical Cyclone Report Hurricane Wilma 15–25 October 2005 2006.
107. J. P. Cangialosi, A. S. Latto, R. Berg, National Hurricane center tropical cyclone report: Hurricane Irma. 2018.
108. G. L. Wingard, S. E. Bergstresser, B. L. Stackhouse, M. C. Jones, M. E. Marot, K. Hoefke, A. Daniels, K. Keller, Impacts of hurricane Irma on Florida Bay Islands, Everglades National Park, USA. *Estuaries Coasts* **43**, 1070–1089 (2020).

Acknowledgments: This project was funded by the Irish Research Council under grant number GOIPD/2022/519 to Y.M. and I.D. Part of the research was conducted at the Jet Propulsion Laboratory, California Institute of Technology, under a contract with the National Aeronautics and Space Administration (NASA, 80NM0018D0004). M.S. was funded by the NASA Land-Cover and Land-Use Change (LCLUC) program. **Author contributions:** Y.M. developed the method, processed the data, and drafted the manuscript. I.D. and J.W.H. conceptualized the study. Y.M. and I.D. led the writing. All authors contributed to analyzing the data and editing the manuscript. **Competing interests:** The authors declare that they have no competing interests. **Data and materials availability:** All data needed to evaluate the conclusions in the paper are present in the paper and/or the Supplementary Materials. The data and scripts to develop the interpretable machine learning model are publicly available via Zenodo (10.5281/zenodo.16779240) and GitHub (https://github.com/moyu-ENV).

Submitted 26 March 2025
Accepted 31 October 2025
Published 5 December 2025
10.1126/sciadv.adx6799